High-Power Recirculating Planar Crossed-Field Amplifier Design and Development

Steven C. Exelby, *Student Member, IEEE*, Geoffrey B. Greening, *Member, IEEE*, Nicholas M. Jordan, *Member, IEEE*, Drew A. Packard, *Student Member IEEE*, David Simon, *Member IEEE*, Y. Y. Lau, *Fellow, IEEE*, Brad W. Hoff, *Member, IEEE*, and Ronald M. Gilgenbach, *Life Fellow, IEEE*

***Abstract*— The recirculating planar crossed-field amplifier (RPCFA) was designed and simulated using the finite-element frequency-domain code ANSYS HFSS and the particle-in-cell (PIC) code MAGIC. The RPCFA is a high-power microwave device adapted from the recirculating planar magnetron, developed at the University of Michigan, Ann Arbor, MI, USA. Electromagnetic (EM) PIC simulations of a planar, meander line, and slow wave structure demonstrated 13.5-dB amplification of a 1.3-MW, 3-GHz signal to approximately 29 MW. The RPCFA is designed to be driven by pulsed power from the Michigan electron long beam accelerator-ceramic insulator, which is currently configured to deliver pulses at −300 kV, 1–10 kA, with 0.3–1 μs pulse lengths. The RF input-drive signal will be provided by an MG5193 magnetron which delivers 5-μs pulses up to 2.6 MW at 3 GHz. EM PIC simulations also demonstrated zero-drive stability of the design and were used to evaluate changes in performance resulting from variations of several experimental parameters. Variation of the drive frequency suggested that the RPCFA is expected to have a 3-dB amplification bandwidth of 300 MHz or 10%.**

***Index Terms*— Crossed-field amplifier (CFA), electron beams, high-power microwave (HPM), MAGIC, particle in cell (PIC), vacuum electronics.**

I. Introduction

THE magnetron is a ubiquitous crossed-field device, with applications ranging from radar communications and counter-electronics to commercial and domestic material heating [1]–[3]. The hallmarks of this device are its compactness, high power, and high efficiency, which are a result of its crossed-field geometry. The recirculating planar magnetron (RPM) [4], [5] is a modification of the standard cylindrical magnetron design with several additional advantages. The increased cathode area allows much higher currents, and the increased anode area allows faster heat dissipation. The recirculating bends allow nearly full beam recirculation, yielding higher efficiency than that of existing planar magnetrons or crossed-field amplifiers (CFAs), some of which require beam dumps. The planar nature of the RPM offers more favorable scaling of the magnetic field volume with number of cavities compared to a cylindrical design, N versus N^2. This feature allows the RPM to retain its compactness even when scaled to high-power applications [6].

A CFA has the same crossed-field interaction as magnetron oscillators for gain, but uses an RF circuit that is terminated at its ends by input and output ports [7]. Like the magnetron, it is notable for its compactness, high efficiency, and capacity for operation at high powers. CFAs are frequently used for shipboard radar and electronic countermeasure systems [8].

The recirculating planar CFA (RPCFA), shown in Fig. 1, retains the advantages of the RPM and is therefore expected to possess similar advantages over cylindrical CFAs. For instance, the length of the amplifying structure can be easily modified to accommodate the requirements of a particular application. The recirculating bends effectively demodulate the beam as each provides a drift space of 180° around the cathode, longer than is generally found in cylindrical CFAs. The planar region opposite the slow wave structure (SWS) can function as a drift space to demodulate the beam further. This demodulation minimizes the electronic feedback which is known to both limit and cause undesirable variations in gain [8]. This geometry is expected to enable amplification of an RF signal to high-power levels typically reserved for other high-power microwave sources [9].

II. Experimental Configuration

The RPCFA is designed to operate at the parameters of the pulsed power source available at the Plasma, Pulsed Power, and Microwave Laboratory, University of Michigan, Ann Arbor, MI, USA. The pulsed power is supplied by Michigan

Manuscript received October 30, 2017; revised December 11, 2017; accepted December 19, 2017. Date of publication January 24, 2018; date of current version May 21, 2018. This work was supported by the Air Force Office of Scientific Research under Grant FA9550-15-1-0097 and Grant FA9550-15-1-0419 and in part by the L-3 Communications Electron Devices. The work of S. C. Exelby was supported in part by the Directed Energy Professional Society, in part by L-3, and in part by AFOSR. The review of this paper was arranged by Editor D. K. Abe. *(Corresponding author: Steven C. Exelby.)*

S. C. Exelby, N. M. Jordan, D. A. Packard, Y. Y. Lau, and R. M. Gilgenbach are with the Department of Nuclear Engineering and Radiological Sciences, University of Michigan, Ann Arbor, MI 48105 USA (e-mail: scexlb@umich.edu; jordann@umich.edu; drupac@umich.edu; yylau@umich.edu; rongilg@umich.edu).

G. B. Greening was with the Department of Nuclear Engineering and Radiological Science, University of Michigan, Ann Arbor, MI 48109 USA. He is now with Communications and Power Industries, Beverly, MA 01915-5536 USA (e-mail: geofgree@umich.edu).

D. Simon and B. W. Hoff are with the Air Force Research Laboratory, Albuquerque, NM 87123 USA (e-mail: david.simon.23@us.af.mil; brad.hoff@us.af.mil).

Color versions of one or more of the figures in this paper are available online at http://ieeexplore.ieee.org.

Digital Object Identifier 10.1109/TED.2018.2790802

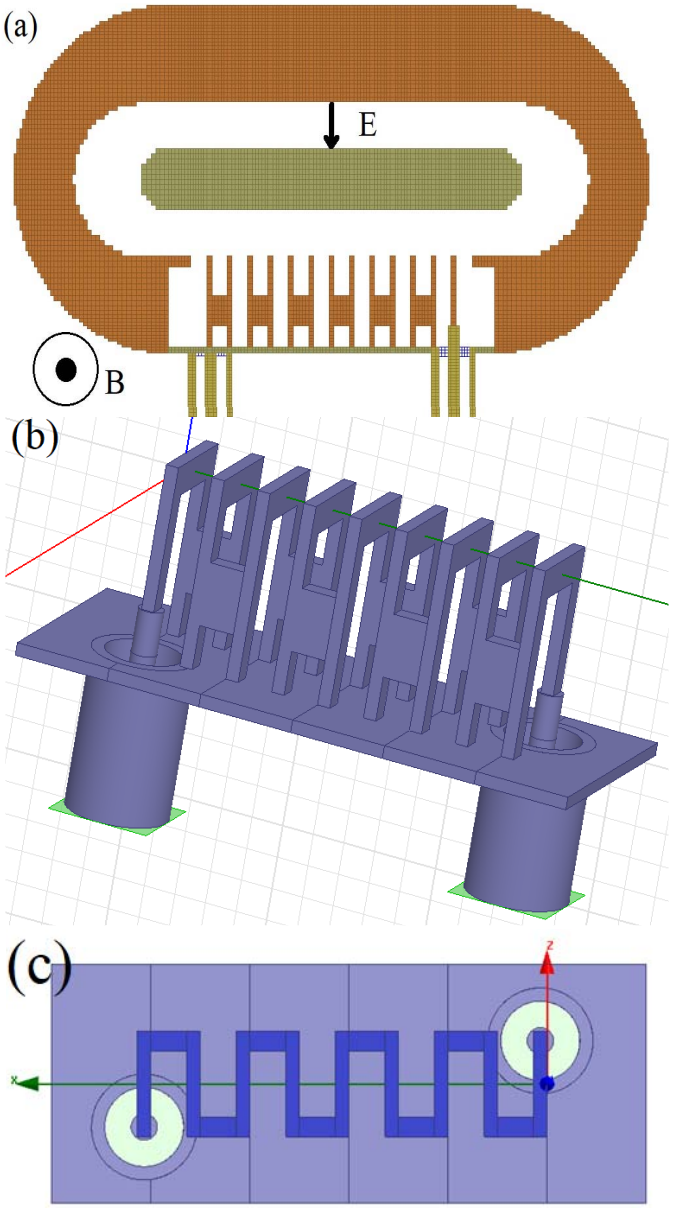

Fig. 1. (a) Axial cross section of the RPCFA developed in MAGIC. The planar cathode is shown in the center with the SWS below it. The coaxial input and extraction ports are shown as they meet with the SWS. (b) SWS developed in ANSYS HFSS shown from an isometric view. (c) Overhead to highlight the meander line structure.

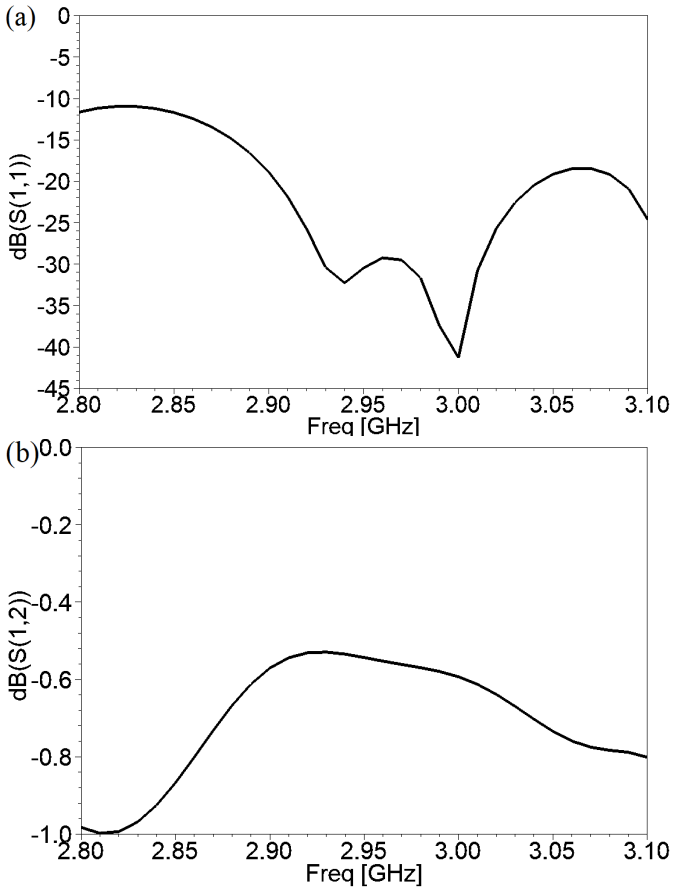

Fig. 2. (a) Plot of simulated S_{11} versus frequency around the 3-GHz design frequency. (b) Plot of simulated S_{12} versus frequency.

electron long beam accelerator-ceramic insulator (MELBA-C), which can provide pulses of −250 to −350 kV at currents of 1–10 kA for up to 1 μs [10]. Pulsed Helmholtz coils provide the axial magnetic field of 0.10–0.32 T. These parameters determine the electrical and physical characteristics of the RPCFA. Chiefly, the device must be large enough to accommodate high electric fields, due to the high voltage supplied to the cathode. In addition, for the Brillouin hub [11], [12] to be synchronous with a slow wave phase velocity of 20%–30% of c, the anode–cathode (AK) gap must be on the order of 1 cm. This restricts the AK gap distance to a narrow range [11].

The RF input signal is provided by a Siemens MG5193 magnetron. This magnetron delivers up to 2.6 MW at a tunable frequency between 2.993 and 3.002 GHz, up to 5-μs pulselength. This fixes the RPCFA frequency at 3 GHz.

III. Simulation of the RPCFA

The SWS for the RPCFA was designed and simulated using ANSYS Electronic Desktop, HFSS driven modal simulations [13]. The structure is shown in Fig. 1(b) and (c) (see also Fig. 9 for a fabricated device). The SWS is a forward wave, rectangular meander line with 202-Ω interaction impedance that couples to coaxial ports on both ends. The coaxial lines ensure a broadband impedance match between the SWS and the surrounding RF circuit. A combination of perfect electrical conducting and radiating boundaries were used in the simulation of the SWS response to the injected signal. Within the passband of the SWS, the type of boundary had a little effect on the electrical characteristics. This result was expected since much of the field energy is carried close to the structure, indicative of minimal radiative energy loss.

The requirement that the RF signal be transmitted with minimal reflection is verified by plotting the simulated scattering parameter S_{11} against frequency as shown in Fig. 2(a). Fig. 2(a) shows that the SWS is well matched to the coaxial input and output at the source RF frequency of 3 GHz.

Plotting S_{12} over frequency as shown in Fig. 2(b) indicates the effectiveness of the SWS as a passive transmission line in the absence of an electron beam; at 3 GHz, 87% of the power

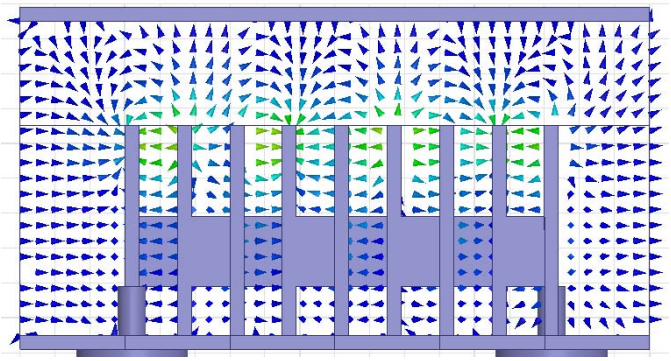

Fig. 3. Side view of the SWS with the HFSS electric field vectors overlaid.

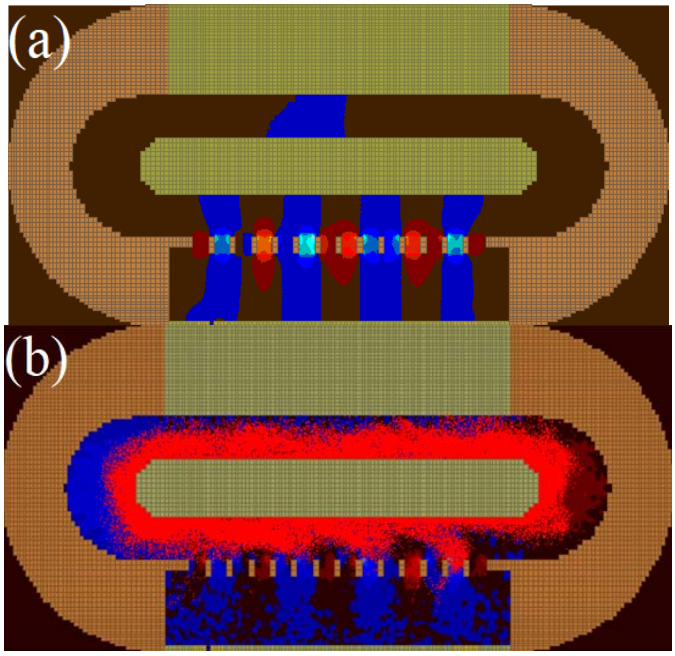

Fig. 4. (a) RF electric field generated in MAGIC when the RPCFA is excited at 3 GHz with no electron beam. Red indicates the field is pointed to the left, blue indicates field is pointed toward the right. (b) Snapshot of EM PIC simulation showing electron spoke formation as the injected signal and the particles (red) move left to right across the SWS.

injected at one end of the SWS is transmitted. Fig. 2(a) and (b) confirms the requirements for high transmission and low reflection for the RPCFA SWS are satisfied.

Two additional requirements for the SWS electric fields are verified by examining the electric fields generated in response to a 3-GHz signal. The field, simulated in HFSS, is displayed in Fig. 3.

The RF electric field changes phase by approximately 90° for every cell of the SWS. Using this information and the SWS cell length of 7.5 mm implies a phase velocity of 30% of the speed of light, a speed slow enough that the Brillouin hub's electrons can synchronously interact with the SWS [11]. The second requirement is that the RF electric field must have a significant component in the Brillouin flow direction so that $\mathbf{E}_{RF} \times \mathbf{B}$ drift provides efficient spoke formation, drawing hub electrons to the anode. The desired fields are shown in Fig. 3.

A 12-cell SWS was modeled in the electromagnetic (EM) particle-in-cell (PIC) code MAGIC [14], [15]. The cathode includes endhats to reduce axial current loss [16], and the anode includes electron beam recirculation bends to accurately

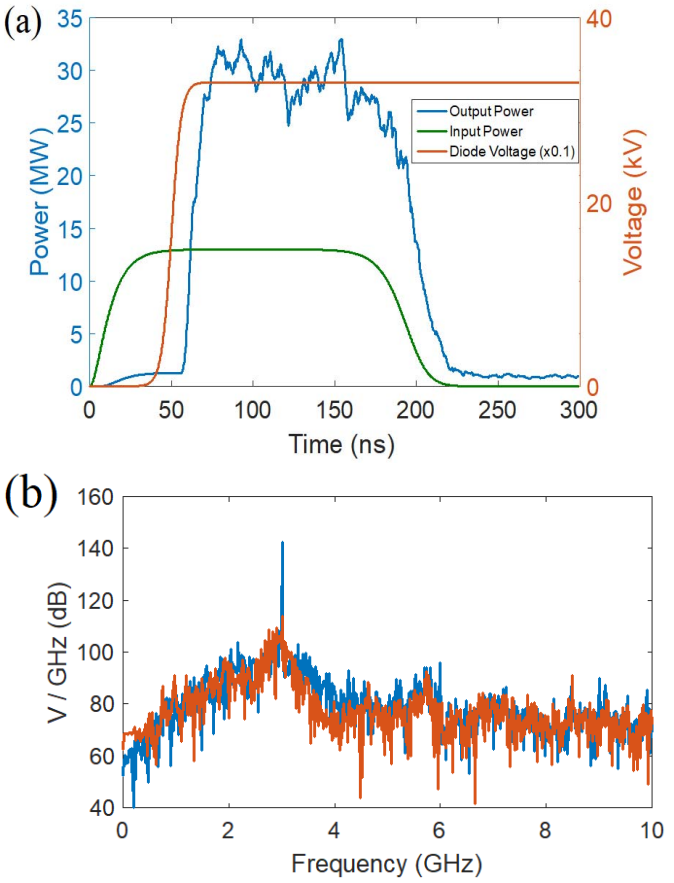

Fig. 5. (a) Simulated output power and the injected signal power over time. (b) FFT traces of the voltage measured across a cell of the SWS. The blue spectrum is taken during amplification, and the red trace is taken once the RF drive is terminated.

perform PIC simulation of a 3-D prototype. A 3-GHz signal was applied at the coaxial input port with no particle emission permitted to verify the cold-tube results from HFSS using the finite-difference time-domain method used in MAGIC. The resulting fields are depicted in Fig. 4.

The EM field structure resulting from the excitation closely matches the field in Fig. 3. In addition, there are minimal losses or reflections of the signal across the length of the 12-cell SWS, which confirms the predictions from HFSS.

A dc voltage of −330 kV and RF power of 1.3 MW were supplied to the RPCFA in MAGIC simulation [14] with a 0.23-T magnetic field. These parameters are nominal values obtainable in the laboratory. Steady-state amplification of the injected signal was achieved on the order of 10 ns following the application of dc power. Spoke formation, indicating the transfer of power from the Brillouin hub electrons to the wave, can be seen in Fig. 4(b).

A net current of 540 A was emitted from the cathode of which 160 A was collected on the SWS. Most of the current not collected at the SWS was collected in the recirculating bends or the planar drift space opposite the SWS. Axial losses were consistently less than 10 A. Microwave power of 29 MW was measured at the output of the RPCFA, giving approximately 13.5-dB gain. The total efficiency, calculated from the total current emission, is thus 15.5%. The electronic efficiency, which includes only the current drawn to the SWS,

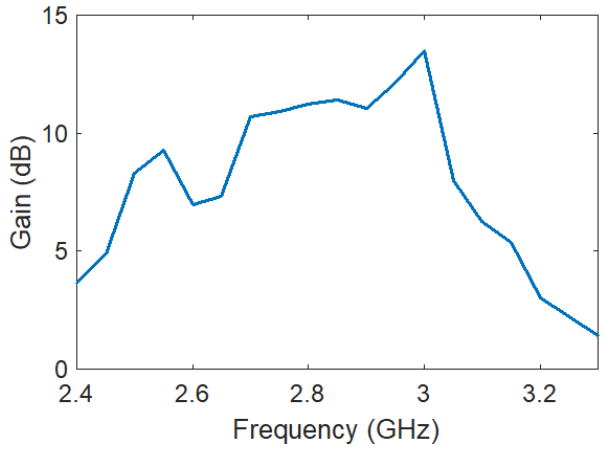

Fig. 6. Simulated gain versus RF drive frequency, showing the bandwidth of the RPCFA.

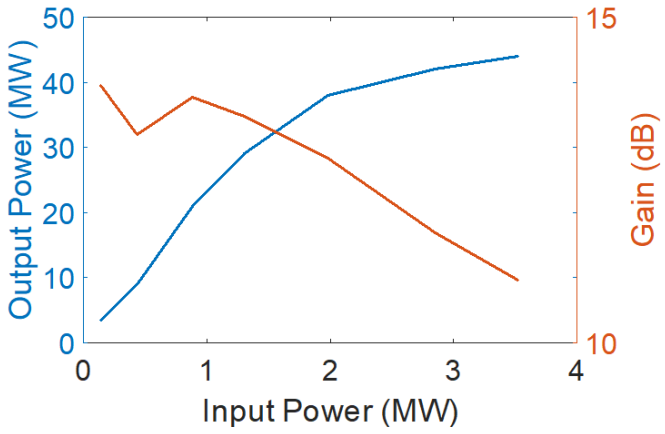

Fig. 7. Simulated output power and gain of the RPCFA as a function of the RF drive power.

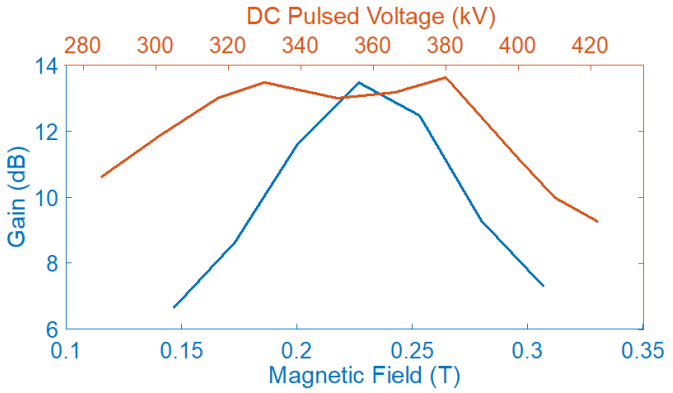

Fig. 8. RPCFA response to variation in the magnetic field strength and the pulsed dc voltage.

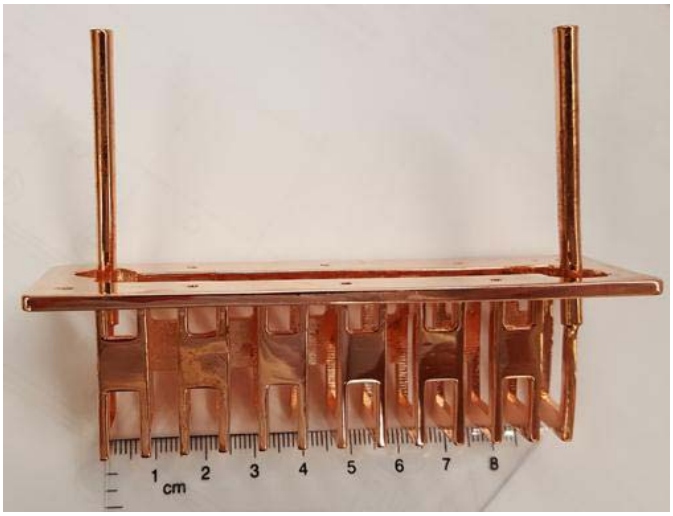

Fig. 9. Copper SWS. The meander line is shown below the extensions which form the inner conductor of the coaxial input–output ports.

is 52%. These efficiencies are acceptable for high-power crossed-field devices though greater efficiencies have been achieved [17].

Zero-drive stability was investigated to confirm the RPCFA amplified an injected signal rather than oscillating at a primed frequency [18]. The RF signal was first injected and then allowed to reach a steady state of propagation on the circuit, at which point the pulsed dc voltage was applied. After reaching steady-state amplification, the RF drive signal was smoothly turned OFF. Simulated output power and the voltage of the driver signal versus time are depicted in Fig. 5(a).

While the lack of appreciable power at the output (after the input RF signal is turned OFF) is evidence of zero-drive stability, nondrive frequency modes may still exist within the RPCFA. The coaxial extraction ports have a limited bandwidth that may prevent signals from reaching the output port. The frequency content inside the amplifier was measured by performing a fast Fourier transform (FFT) of the voltage across a cell located toward the output end of the SWS. The FFT was performed both during amplification and after the RF signal was terminated. The two spectra are presented in Fig. 5(b).

The spectra confirm the zero-drive stability of the RPCFA. No frequency is amplified other than the 3-GHz RF drive. Furthermore, once the RF drive is terminated, the spectrum does not change significantly and no frequency persists within the RPCFA significantly above the noise floor.

A sweep over relevant parameters was performed to characterize the RPCFA as shown in Figs. 6 and 7. The frequency of the injected signal was varied to measure the bandwidth of the device (Fig. 6). A gain of $\geq$10 dB was observed over a continuous range from 2.7 to 3 GHz. This is comparable with commercial CFAs [19].

The power of the injected RF signal was varied to calculate the gain and output power as a function of the input power, as shown in Fig. 7. The gain tended to decrease as the drive power was increased though the output power monotonically increased. Nearly, a 45 MW of RF power was generated at the highest drive power, at the cost of gain and efficiency.

The RPCFA's response to suboptimal magnetic field strength was also simulated. The initial simulations of the RPCFA used a magnetic field strength calculated from the Buneman–Hartree condition and a pulsed dc voltage of 330 kV. It was determined by varying the magnetic field that the Buneman–Hartree condition accurately predicted the optimal performance of the RPCFA with a peak at 0.23 T, as shown in Fig. 8. Similarly, the pulsed dc voltage of the pulsed power driving the RPCFA was varied, holding the magnetic field constant at 0.23 T, to examine its effect on RPCFA performance. It was found that output power tended to increase with slightly greater applied voltage, though this came at the cost of

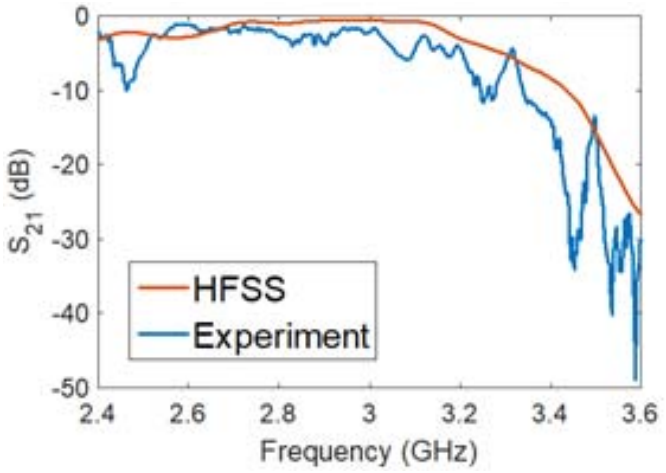

Fig. 10. S_{21} generated from HFSS and measured experimentally using the prototype.

efficiency. Lower voltages had uniformly inferior performance. Gain was greater than 10 dB for pulsed dc voltages between 285 and 400 kV. These results are summarized in Fig. 8.

IV. Fabrication of the RPCFA

After simulations in MAGIC and HFSS converged on an acceptable and well characterized design, the RPCFA was fabricated. Due to its small size and relative complexity, the copper SWS was fabricated using a 3-D printing-assisted lost wax casting process [20]. The resulting SWS is shown in Fig. 9. Other components of the RPCFA, including the cathode, the housing with recirculating bends, coaxial to rectangular waveguide couplers, and the fixtures to center the RPCFA in the vacuum chamber were machined from aluminum. The cathode will be made from aluminum. Velvet emitters will be applied where emission is encouraged, over the SWS, and the remainder of the cathode will be coated in glyptal to reduce emission from undesired locations.

With the assembly constructed and installed, a cold test was performed in order to verify the quality of construction and determine the validity of simulations. A comparison between the HFSS simulated S_{21} and the experimental measurement is depicted in Fig. 10.

While the curves qualitatively agree, the experimental curve reveals uniformly higher loss across the tested frequencies. Tuning stubs were later added to the experimental cold test to minimize potential impedance mismatches. It was found that the stubs were unable to improve the match near the design frequency, which suggests the sources of losses are resistive and radiative. Resistive losses were not considered in simulation as perfect conductors were used and electrical contact resistance was ignored. At 3 GHz, S_{21} is approximately -1.9 dB suggesting 65% of the RF power is transmitted, an acceptable level of loss which should not lead to significant deterioration of performance according to MAGIC PIC simulations.

V. Conclusion

The RPCFA is a novel adaption of the RPM concept to a CFA-type device. This paper has outlined the principles behind the development of the device as well as the results of simulations predicting the behavior of a functioning RPCFA. The fabrication of the prototype has been presented and the experimental cold test suggests that the experiment reproduces the design developed in simulation.

Future research will investigate the performance of the prototype as a viable high-power CFA. The gain and bandwidth of the RPCFA will be determined experimentally as will the device's response to changes in the applied electric and magnetic fields. Zero-drive stability has already been verified on the MELBA-C generator.

References

[1] T. A. Spencer, "Current HPM source research," in *Proc. 6th Workshop High Energy Density High Power RF*, Berkeley Springs, WV, USA, 2003, p. 46.
[2] G. B. Collins, *Microwave Magnetrons*. New York, NY, USA: McGraw-Hill, 1948.
[3] R. M. Gilgenbach, Y. Y. Lau, H. McDowell, K. L. Cartwright, and T. A. Spencer, *Modern Microwave and Millimeter-Wave Power Electronics* (Crossed-Field Devices), R. J. Barker, N. C. Luhmann, J. H. Booske, and G. S. Nusinovich, Eds. Piscataway, NJ, USA: IEEE Press, 2004.
[4] R. M. Gilgenbach, Y. Y. Lau, D. M. French, B. W. Hoff, J. Luginsland, and M. Franzi, "Crossed field device," U.S. Patent US 8 841 867 B2, Sep. 23, 2014.
[5] R. M. Gilgenbach, Y.-Y. Lau, D. M. French, B. W. Hoff, M. Franzi, and J. Luginsland, "Recirculating planar magnetrons for high-power high-frequency radiation generation," *IEEE Trans. Plasma Sci.*, vol. 39, no. 4, pp. 980–987, Apr. 2011.
[6] M. A. Franzi *et al.*, "Recirculating-planar-magnetron simulations and experiment," *IEEE Trans. Plasma Sci.*, vol. 41, no. 4, pp. 639–645, Apr. 2013.
[7] W. C. Brown, "The history of the reentrant beam crossed field amplifier with emphasis on noise comparison with the magnetron," in *Proc. 1st Int. Workshop Crossed-Field Devices*. Ann Arbor, MI, USA, 1995, pp. 9–22.
[8] A. S. Gilmour, *Klystrons, Traveling Wave Tubes, Magnetrons, Crossed-Field Amplifiers, and Gyrotrons*. Norwood, MA, USA: Artech House, 2011, pp. 543–581.
[9] J. A. Benford, J. A. Swegle, and E. Schamiloglu, *High Power Microwaves*. Boca Raton, FL, USA: CRC Press, 2007.
[10] M. R. Lopez *et al.*, "Relativistic magnetron driven by a microsecond E-beam accelerator with a ceramic insulator," *IEEE Trans. Plasma Sci.*, vol. 32, no. 3, pp. 1171–1180, Jun. 2004.
[11] D. H. Simon, Y. Y. Lau, G. Greening, P. Wong, B. Hoff, and R. M. Gilgenbach, "Stability of Brillouin flow in the presence of slow-wave structure," *Phys. Plasmas*, vol. 23, no. 9, p. 092101, 2016.
[12] Y. Y. Lau *et al.*, "A re-examination of the Buneman–Hartree condition in a cylindrical smooth-bore magnetron," *Phys. Plasmas*, vol. 17, no. 3, p. 033102, Mar. 2010.
[13] *Ansys HFSS*. Accessed: May 1, 2014. [Online]. Available: http://www.ansoft.com/products/hf/hfss/
[14] *MAGIC Electromagnetic-PIC Software*, Alliant Techsyst. (ATK), Newington, VA, USA, 2014.
[15] R. W. Lemke, T. C. Genoni, and T. A. Spencer, "Three-dimensional particle-in-cell simulation study of a relativistic magnetron," *Phys. Plasmas*, vol. 6, no. 2, pp. 603–613, Feb. 1999.
[16] R. W. Lemke, T. C. Genoni, and T. A. Spencer, "Effects that limit efficiency in relativistic magnetrons," *IEEE Trans. Plasma Sci.*, vol. 28, no. 3, pp. 887–897, Jun. 2000.
[17] M. I. Fuks and E. Schamiloglu, "70% efficient relativistic magnetron with axial extraction of radiation through a horn antenna," *IEEE Trans. Plasma Sci.*, vol. 38, no. 6, pp. 1302–1312, Jun. 2010.
[18] J. Benford, H. Sze, W. Woo, R. R. Smith, and B. Harteneck, "Phase locking of relativistic magnetrons," *Phys. Rev. Lett.*, vol. 62, no. 8, pp. 969–971, Feb. 1989.
[19] L-3 Communications Holdings, Inc. (2015). *Crossed-Field Amplifiers*. [Online]. Available: http://www2.l-3com.com/edd/products/r_cfas.htm
[20] Materialise NV. (2017). *Lost Wax Printing and Casting*. [Online]. Available: https://i.materialise.com/3d-printing-technologies/lost-wax-printing-casting

Authors' photographs and biographies not available at the time of publication.